Geophysical Journal International

Geophys. J. Int. (2017) **210,** 255–269
Advance Access publication 2017 April 24
GJI Geomagnetism, rock magnetism and palaeomagnetism

doi: 10.1093/gji/ggx153

Experimental test of the heating and cooling rate effect on blocking temperatures

Thomas Berndt,[1] Greig A. Paterson,[2] Changqian Cao[2,3] and Adrian R. Muxworthy[1]

[1] *Department of Earth Science and Engineering, Imperial College London,* SW7 2AZ, *United Kingdom. E-mail: t.berndt13@imperial.ac.uk*
[2] *Key Laboratory of Earth and Planetary Physics, Institute of Geology and Geophysics, Chinese Academy of Sciences, Beijing* 100029, *China*
[3] *France-China Bio-Mineralization and Nano-Structures Laboratory, Chinese Academy of Sciences, Beijing* 100029, *China*

Accepted 2017 April 19. Received 2017 March 27; in original form 2016 October 21

SUMMARY

The cooling rates at which rocks acquire thermoremanent magnetizations (TRMs), affect their unblocking temperatures in thermal demagnetization experiments; similarly the heating rates at which the thermal demagnetization experiments are done also affect the unblocking temperature. We have tested the effects of variable cooling and heating rates on the unblocking temperatures of two natural non-interacting, magnetically uniform (single-domain, SD) (titano)magnetite samples and a synthetic SD magnetoferritin sample. While previous studies have only considered unblocking temperatures for stepwise thermal demagnetization data (i.e. the room-temperature magnetization after incremental heating), in this work we derive an expression for continuous thermal demagnetization of both TRMs and viscous remanent magnetizations (VRMs) and relate the heating rate to an effective equivalent hold time of a stepwise thermal demagnetization experiment. Through our analysis we reach four main conclusions: First, the theoretical expressions for the heating/cooling rate effect do not accurately predict experimentally observed blocking temperatures. Empirically, the relation can be modified incorporating a factor that amplifies both the temperature and the heating rate dependence of the heating/cooling rate effect. Using these correction factors, Pullaiah nomograms can accurately predict blocking temperatures of both TRMs and VRMs for continuous heating/cooling. Second, demagnetization temperatures are approximately predicted by published 'Pullaiah nomograms', but blocking occurs gradually over temperature intervals of 5–40 K. Third, the theoretically predicted temperatures correspond to ∼54–82 per cent blocking, depending on the sample. Fourth, the blocking temperatures can be used to obtain estimates of the atomic attempt time τ_0, which were found to be 3×10^{-10} s for large grained (titano)magnetite, 1×10^{-13} s for small grained (titano)magnetite below the Verwey transition and 9×10^{-10} s for magnetoferritin (∼8 nm).

Key words: Magnetic mineralogy and petrology; Palaeointensity; Palaeomagnetism applied to geologic processes; Rock and mineral magnetism.

1 INTRODUCTION

When magnetic minerals cool from above their Curie temperature T_C in the Earth's magnetic field they acquire a thermoremanence (TRM). At temperatures just below T_C, the intrinsic magnetic energies can be easily overcome by thermal fluctuations, and the magnetic moment of a crystal is free to move between local energy minima. On cooling to ambient temperature, there comes a point where the thermal fluctuations are no longer sufficient to overcome the energy barriers to other states. The magnetization is then frozen in a particular configuration and is referred to as being blocked. Accurate estimation of blocking temperatures plays an important role in palaeomagnetism, for example, in the determination of emplacement temperatures of pyroclastic deposits (Paterson *et al.* 2010) and viscous remanent magnetization (VRM) dating (Berndt & Muxworthy 2017). Using Néel's (1949) theory of magnetic single-domain (SD) particles, Pullaiah *et al.* (1975) plotted nomograms of the blocking condition derived for demagnetization temperatures determined in stepwise thermal demagnetization experiments to acquisition times and temperatures. Here, stepwise heating refers to the standard procedure of measuring the room-temperature magnetic remanence after heating to a given temperature in zero-field. Experimental tests of this relationship are generally positive (e.g. Dunlop & Özdemir 1993, 2000; Jackson & Worm 2001), though sometimes higher demagnetization temperatures have been observed (Dunlop 1983; Kent 1985; Kent & Miller 1987); these

discrepancies are attributed to the response of larger pseudo-SD (PSD) and/or multidomain (MD) grains (Dunlop & Özdemir 2000), but more experimental evidence is needed.

As Pullaiah nomograms relate acquisition times and temperatures to demagnetization times and temperatures, they strictly only apply to VRMs that are acquired at a constant temperature T_A over a finite time t_A and to stepwise thermal demagnetization where a temperature T_D is held constant over a time t_D. TRMs, however, are acquired during continuous cooling of a rock and therefore do not have a constant acquisition temperature. York (1978a,b) and Dodson & McClelland-Brown (1980) derived relationships between the cooling rate r_A at which a TRM is acquired, the demagnetization temperature, and time during stepwise thermal demagnetization. Experimental confirmation of their equations are, however, difficult because they rely on accurate knowledge of the cooling rates of geological samples, and stepwise thermal demagnetization experiments do not allow for a high temperature accuracy to measure the cooling rate effect at high precision. Walton (1980) derived an alternative expression to the one used by Pullaiah *et al.* (1975), to relate acquisition and demagnetization times and temperatures taking into account their grain-size distributions. Enkin & Dunlop (1988), however, pointed out that Walton's relation answer a different question than Pullaiah's: they relate temperatures/times to produce equal total magnetic moments (i.e. palaeointensities), while Pullaiah describes what temperature is necessary to fully demagnetize (or re-magnetize) a given magnetic component (i.e. activate the same set of grains). Both expressions are valid and useful, however, for the study of blocking temperatures only Pullaiah's equation is relevant. Many studies have investigated the effect of cooling rates on TRMs, but largely focussed on their influence on palaeointensity determinations rather than blocking temperatures (Fox & Aitken 1980; Halgedahl *et al.* 1980; McClelland-Brown 1984; Williams & Walton 1988; Ferk *et al.* 2010; Muxworthy & Heslop 2011; Muxworthy *et al.* 2011; Biggin *et al.* 2013; Muxworthy *et al.* 2013).

The converse of this cooling rate problem, is that of thermal demagnetization by continuous heating: continuous thermal demagnetization (CTD) is a technique by which the temperature of a sample is continuously increased while measuring the three components of its remanent magnetic moment as a function of temperature (Creer 1967). This permits the determination of palaeodirections (Schmidt & Clark 1985; Dunlop 2009), Thellier & Thellier (1959) and Wilson (1961) type palaeointensity experiments (Le Goff & Gallet 2004) and the dating of viscous overprints (VRM dating) caused by events such as floods (Muxworthy *et al.* 2015). Advantages of CTD include minimal sample handling, full automation, reduction of heating cycles compared to stepwise thermal demagnetization and a high temperature resolution, the latter of which is essential for VRM dating (Berndt & Muxworthy 2017). For stepwise thermal demagnetization, blocking temperatures can be interpreted using Pullaiah nomograms with the timescale t_D, the time the temperature is held constant in the thermal demagnetizer. In CTD, however, an expression is needed to relate blocking temperatures to the heating rate r_D rather than the hold time.

The aim of this study is twofold: first, to provide more direct experimental evidence for Pullaiah nomograms using well characterized SD samples. Second, an expression relating heating rate to blocking temperatures based on the ideas of York (1978a,b) is derived and experimentally tested using CTD to demagnetize previously induced VRMs and pTRMs of known acquisition times and temperatures. This expression would play an important role in interpreting palaeomagnetic data obtained from CTD experiments.

2 REVIEW OF THE COOLING RATE EFFECT

According to Néel (1949) theory of identical SD particles, the net magnetic moment n (i.e. the number of magnetic moments that are aligned with the applied field minus the number of magnetic moments that are in the opposite direction), approaches its equilibrium value n_{eq} according to the differential equation

$$\frac{\mathrm{d}n}{\mathrm{d}t} = \frac{n_{eq} - n}{\tau}\,, \tag{1}$$

where t is time and τ the relaxation time. For fields larger than about 0.3 mT for magnetite (Néel 1949), τ is given by

$$\frac{1}{\tau} = \frac{1}{\tau_0}\exp\left\{-\frac{\varepsilon\,(T)}{kT}\left(1 - \frac{|H_0|}{H_K}\right)^2\right\}\,, \tag{2}$$

where τ_0 is the atomic attempt time, ε is the energy barrier for coherent rotation of an SD magnetic moment, k is the Boltzmann constant, T is temperature, H_0 is the externally applied magnetic field, and H_K is the microscopic coercive force. For weak fields, the relaxation time is given by (Néel 1949)

$$\frac{1}{\tau} = \frac{2}{\tau_0}\exp\left\{-\frac{\varepsilon\,(T)}{kT}\right\}\,. \tag{3}$$

From this, it can been seen that the magnetization changes gradually rather than blocks instantaneously. York (1978a,b) derived an expression for the time at which the net magnetization has reached a proportion p of its equilibrium value (e.g. 95 per cent) by integrating eq. (3). He showed that if the temperature is a function of time, $T(t)$, and the spontaneous magnetization is given by the analytical approximation for magnetite,

$$M_s\,(T) = M_{s0}\sqrt{1 - \frac{T}{T_C}}\,, \tag{4}$$

where M_{s0} is the spontaneous magnetization at room temperature and T_C is the Curie temperature, then the expression for τ in eq. (3) can be rewritten as

$$\frac{\varepsilon\,(T)}{kT} = \ln\left(\frac{2\gamma kT\,(1 - T/T_C)}{\tau_0 \dot{T}\varepsilon \ln p}\right)\,, \tag{5}$$

where $\ln\gamma \approx 0.577$ is Euler's constant and $\dot{T}$ is the time derivative of the temperature. York (1978a,b) calculated $p = 5$ per cent and 95 per cent blocking intervals. If p is set to $e^{-1} \approx 0.37$, corresponding to the time/temperature at which blocking is 37 per cent complete, the $\ln(p)$ term inside the brackets vanishes. Compared to the concept of blocking by Néel (1949), defined by the relaxation time $t \approx \tau$: for a constant temperature, eq. (1) predicts a net magnetization of

$$n\,(t) = n_0 e^{-t/\tau} + n_{\mathrm{eq}}\left(1 - e^{-t/\tau}\right)\,, \tag{6}$$

to retain 37 per cent of its initial magnetization during blocking.

Differing from Néel's concept of a blocking temperature where the relaxation time is equal to the experimental time, Dodson (1976) defined the blocking temperature T_B to be the temperature at which the thermodynamic equilibrium magnetization is equal to the 'frozen-in' value of the rock. The slower the cooling rate, the more time the grains have to get closer to thermodynamic equilibrium; slower cooling rates will lead to higher temperatures necessary for subsequent demagnetization. In Dodson & McClelland-Brown (1980), an expression building on this theory is derived that relates the blocking temperature of a slowly cooling rock to the unblocking temperature during thermal demagnetization at constant

temperature (as an approximation to stepwise demagnetization). They defined a cooling time constant θ,

$$\frac{1}{\theta} = \frac{1}{kT}\left(\frac{\mathrm{d}\varepsilon}{\mathrm{d}T} - \frac{\varepsilon}{T}\right)\dot{T}\,, \tag{7}$$

which, for magnetite dominated by shape anisotropy, becomes

$$\theta = \frac{kT^2\,(1 - T/T_C)}{(-\dot{T})\,\varepsilon}\,. \tag{8}$$

After integration with the boundary condition of $n(T(t))$ approaching $n_{\mathrm{eq}}(T_B)$ at infinite time, eq. (8) yields a blocking temperature that is given by

$$\frac{\varepsilon\,(T_B)}{kT_B} = \ln\left(\frac{\gamma\theta}{\tau_0}\right)\,, \tag{9}$$

which is equivalent to eq. (5) within a factor of two, which is due to a weak field assumption made by (York 1978a,b).

3 DERIVATION FOR CONTINUOUS HEATING

Largely following the ideas of York (1978a,b), we derive an expression for the demagnetization temperature in the converse problem of continuous heating rather than continuous cooling. As continuous heating experiments are most conveniently done at a constant heating rate r, the temperature at any time t is given by

$$T\,(t) = T_0 + rt\,, \tag{10}$$

where T_0 is the initial temperature (typically room temperature). In the case of demagnetization, the field is zero and hence eq. (1) becomes

$$\frac{\mathrm{d}n}{\mathrm{d}t} = -\frac{n}{\tau}\,, \tag{11}$$

which, inserting the relaxation time from eq. (3) gives

$$\frac{\mathrm{d}n}{\mathrm{d}t} = -\frac{2n}{\tau_0}\exp\left\{-\frac{\varepsilon\,(T)}{kT}\right\}\,. \tag{12}$$

This differential equation has to be integrated in order to obtain the remaining normalized magnetization n, relative to the initial normalized magnetization n_0,

$$\ln(p) = -\frac{2}{\tau_0}\int_{t_0}^{t}\exp\left\{-\frac{\varepsilon\,(T)}{kT}\right\}\mathrm{d}t\,, \tag{13}$$

where $p = n/n_0$. Substituting t for T by means of eq. (10), eq. (13) can be expressed as

$$\ln(p) = -\frac{2}{r\tau_0}\int_{T_0}^{T}\exp\left\{-\frac{\varepsilon\,(T)}{kT}\right\}\mathrm{d}T\,. \tag{14}$$

By using the analytic $M_s(T)$ approximation for magnetite (eq. 4) with shape anisotropy ($H_K(T) \propto M_s(T)$), this becomes

$$\begin{aligned}\ln(p) &= -\frac{2}{r\tau_0}\int_{T_0}^{T}\exp\left\{-\frac{\varepsilon_0}{k}\left(\frac{1}{T} - \frac{1}{T_C}\right)\right\}\mathrm{d}T \\ &= -\frac{2}{r\tau_0}e^{\varepsilon_0/kT_C}\int_{T_0}^{T}\exp\left\{-\frac{\varepsilon_0}{kT}\right\}\mathrm{d}T\,,\end{aligned} \tag{15}$$

where ε_0 is the energy barrier at room temperature. The integration then results in the expression

$$\begin{aligned}\ln(p) = -\frac{2}{r\tau_0}e^{\varepsilon_0/kT_C}\Bigg[&\frac{\varepsilon_0}{k}\mathrm{Ei}\left(-\frac{\varepsilon_0}{kT}\right) - \frac{\varepsilon_0}{k}\mathrm{Ei}\left(-\frac{\varepsilon_0}{kT_0}\right) \\ &+ Te^{-\varepsilon_0/kT} - T_0e^{-\varepsilon_0/kT_0}\Bigg]\,,\end{aligned} \tag{16}$$

where Ei is the exponential integral. In this equation, the two terms containing T_0 are much smaller than the respective terms involving T, and so we can neglect them. The simplified equation is

$$\ln(p) = -\frac{2T}{r\tau_0}e^{\varepsilon_0/kT_c}\left[\frac{\varepsilon_0}{kT}\mathrm{Ei}\left(-\frac{\varepsilon_0}{kT}\right) + e^{-\varepsilon_0/kT}\right]\,. \tag{17}$$

As ε_0/kT is somewhere in the range of 25 to 60 for grains with relaxation times between laboratory and geological time scales, we can use the first two terms of a divergent series to approximate the exponential integral

$$\mathrm{Ei}\,(x) \approx \frac{e^{-x}}{x} + \frac{e^{-x}}{x^2} + \cdots\,. \tag{18}$$

The first term of this series then cancels with the second term in (17). The equation then simplifies to

$$\ln(p) = -\frac{2T}{r\tau_0}\cdot\frac{kT}{\varepsilon_0}\exp\left\{-\frac{\varepsilon_0}{k}\left(\frac{1}{T} - \frac{1}{T_C}\right)\right\}\,. \tag{19}$$

In a similar way that p in eq. (5) is the ratio of the magnetization to its equilibrium value (York 1978a,b), in eq. (19) p is the ratio of the magnetization to its initial value. According to the blocking condition $t \approx \tau$, the demagnetization temperature T_D can then be defined as the temperature where the ratio n/n_0 corresponds to an intensity decay by a factor of e (i.e. $p = e^{-1}$),

$$\frac{\varepsilon_0}{k}\exp\left\{\frac{\varepsilon_0}{k}\left(\frac{1}{T_{D,\mathrm{continuous}}} - \frac{1}{T_C}\right)\right\} = \frac{2T_{D,\mathrm{continuous}}^2}{r\tau_0}\,, \tag{20}$$

where the subscript 'continuous' has been added to make clear that this expression refers to continuous heating experiments. The temperature necessary to demagnetize the same set of grains (described by their room-temperature energy barrier of ε_0) will in general be different in continuous and in stepwise thermal demagnetization experiments, that is, the temperature $T_{D,\,\mathrm{stepwise}}$ will in general differ from $T_{D,\,\mathrm{continuous}}$. Repeating the same calculation for a constant temperature $T_{D,\,\mathrm{stepwise}}$ held over a time interval t_D yields an analogous expression for stepwise thermal demagnetization. As the integrand in eq. (13) is independent of time, this can be expressed as

$$\ln(p) = -\frac{2t_D}{\tau_0}\exp\left\{-\frac{\varepsilon_0}{k}\left(\frac{1}{T_{D,\mathrm{stepwise}}} - \frac{1}{T_C}\right)\right\}\,. \tag{21}$$

Again, setting $p = e^{-1}$ and solving for the activation energy yields

$$\varepsilon_0 = \frac{k}{\left(\frac{1}{T_{D,\mathrm{stepwise}}} - \frac{1}{T_C}\right)}\ln\left\{\frac{2t_D}{\tau_0}\right\}\,. \tag{22}$$

For convenience, we now introduce the concept of an effective relaxation time t_{eff}. We define this to be the hold time of a stepwise demagnetization experiment at temperature T that is necessary to activate (demagnetize) the same grains that are activated as in a continuous heating experiment up to temperature T. In other words, the effective relaxation time corresponds to the hold time such that $T_{D,\,\mathrm{stepwise}} = T_{D,\,\mathrm{continuous}} = T$. By inserting this into eq. (20) one obtains an expression

$$\frac{2t_{\mathrm{eff}}}{\tau_0}\ln\left(\frac{2t_{\mathrm{eff}}}{\tau_0}\right) = \frac{2T}{r\tau_0}\left(1 - \frac{T}{T_C}\right)\,. \tag{23}$$

The effective relaxation time t_{eff} is a theoretical concept that makes it possible to easily interpret data from CTD experiments on Pullaiah diagrams: Traditionally, Pullaiah diagrams can only show constant demagnetization temperatures with finite hold times, which is only applicable to stepwise demagnetization. If one performed a CTD experiment, however, one can simply plot the demagnetization time together with the effective time (calculated from the heating rate,

which is known). This allows to then obtain information about acquisition times and temperatures for CTD in exactly the same way as one would with stepwise thermal demagnetization data.

The equation can either be solved iteratively, or we can make use of the Lambert W function, which is defined as the solution of $x = W(x)e^{W(x)}$. Then the effective time can be written as

$$t_{\rm eff} = \frac{\tau_0}{2} \exp\left\{ W\left(\frac{2T}{r\tau_0}\left(1 - \frac{T}{T_C}\right)\right)\right\} . \tag{24}$$

To get an intuitive understanding of the shape of this function, one can use $W(x) \approx \ln(x) - \ln(\ln(x)) + O(1)$ to obtain the first order approximation

$$t_{\rm eff} = \frac{T}{r}\left(1 - \frac{T}{T_C}\right) \Bigg/ \ln\left(\frac{2T}{r\tau_0}\left(1 - \frac{T}{T_C}\right)\right) . \tag{25}$$

This shows that the effective time is approximately inversely proportional to the heating rate. For illustration purposes, let us consider a simple numerical example: assume a magnetite sample ($T_C = 580\,^\circ$C) is heated at a rate of $r = 1\,^\circ$Cs^{-1} and is demagnetized at 300 °C. The effective time is then (assuming $\tau_0 = 10^{-9}$ s) $t_{\rm eff} = 8$ s. Intuitively speaking, while it takes about 280 s to heat the sample from room temperature up to 300 °C, it is only the final 8 s that really demagnetize the sample. In other words, if the sample was heated instantaneously to 300 °C, one would have to hold the temperature for only 8 s (rather than 280 s) to demagnetize it.

Note that in comparison with eq. (9) the product $\gamma\theta$ can be considered an effective time in the theory of Dodson & McClelland-Brown (1980), which would yield the same expression as eq. (24), up to the factor γ in the Lambert W function.

Pullaiah nomograms are given by (Pullaiah *et al.* 1975)

$$\frac{T_A \ln(2t_A/\tau_0)}{1 - (T_A/T_C)} = \frac{T_D \ln(2t_D/\tau_0)}{1 - (T_D/T_C)} , \tag{26}$$

which follows directly from eq. (3) for weak fields (under the assumption of shape anisotropy and eq. 4) and relates acquisition time t_A and temperature T_A to demagnetization time t_D and temperature. Strictly, Pullaiah nomograms are derived for remanence acquisition/demagnetization at constant temperatures, which is equivalent to VRM acquisition/viscous decay or remanence. Pullaiah nomograms have, however, often been employed to analyse thermoremanent magnetizations (TRMs), for example, to relate demagnetization temperatures from stepwise thermal demagnetization (strictly a viscous process, as it occurs at constant temperature) to approximate TRM acquisition times (strictly a continuous cooling process and hence not applicable to Pullaiah nomograms). By replacing t_D by $t_{\rm eff}$ (eq. 24), Pullaiah-style nomograms can be extended to CTD (continuous heating process).

4 SAMPLES

Three samples were used for the experiments: Two Tiva Canyon Tuff samples provided by the Institute of Rock Magnetism (IRM) of the University of Minnesota and a magnetoferritin sample produced at the Institute of Geology and Geophysics, Chinese Academy of Sciences (IGGCAS) in Beijing. These are well characterized samples that contain almost exclusively SD or SP (titano)magnetite grains, which, at low temperatures, can be used to explore SD behaviour. Due to ageing, the magnetoferritin sample may have oxidized to maghemite.

4.1 Tiva Canyon Tuff

Samples from the Tiva Canyon Tuff have previously been described by Jackson *et al.* (2006), Till *et al.* (2011) and others (Schlinger *et al.* 1988, 1991; Rosenbaum 1993; Worm & Jackson 1999; Egli 2002; Shcherbakov & Fabian 2005). These samples contain mostly non-interacting SD grains of slightly impure magnetite of narrow grain-size distributions, although the larger grained samples may contain PSD grains (Till *et al.* 2011). The impurities are around 10 per cent (TM10) and are mainly Ti, Mn and Cr (Jackson *et al.* 2006). The two samples, TC04-12-01 and TC04-12-07 (12-01 and 12-07, respectively) originate from two different layers of the Tiva Canyon. As described by Till *et al.* (2011), the grain-size varies with stratigraphic height, from approximately 15 nm in length at the base of the Canyon to about 1000 nm at the top. Sample 12-01 is from one of the bottom layers (i.e. containing the smallest and therefore purely SD), and 12-07 is from a higher layer (i.e. containing the largest grains employed for this study, and may contain PSD grains). The samples were crushed into a powder and filled into gel capsules for the experiments. The grain-sizes of various samples of the Tiva Canyon Tuff have been investigated by various different studies and methods: direct observation by transmission electron microscopy (TEM) by Schlinger *et al.* (1991), thermal demagnetization of an isothermal remanent magnetization (IRM) or TRM (Worm & Jackson 1999), frequency-dependent susceptibility analysis (Shcherbakov & Fabian 2005), thermal fluctuation tomography (Jackson *et al.* 2006), viscous decay of an IRM (Berndt *et al.* 2015). Grain-sizes are estimated from TEM (Schlinger *et al.* 1991) to be around 85 nm with a width/length ratio of 0.11 for the larger-grained samples (like 12-07) and around 15 nm with a width/length ratio of 0.36 for the fine-grained samples (like 12-01). Curie temperatures were determined from spontaneous magnetization $M_s(T)$ curves to be 514 °C (12-07) and 471 °C (12-01), respectively, and the atomic attempt time τ_0 was determined to be about 2×10^{-9} s (12-07) and 4×10^{-10} s (12-01), respectively (Berndt *et al.* 2015).

4.2 Magnetoferritin

Magnetoferritin are an ideal material for the study of magnetic properties of non-interacting, randomly oriented, SP ferrimagnetic particles (Cao *et al.* 2010, 2014). Magnetoferritins are nanometre-sized magnetic particles that are individually surrounded by a spherical protein shell, the human H chain ferritin, with an outer diameter of 12–13 nm and an inner diameter of ∼8 nm to prevent the particles from clustering. Through size exclusion chromatography, narrow grain size distributions can be created with well controlled mean sizes (Cai *et al.* 2015).

The magnetoferritin sample used in this study was produced as described in Cao *et al.* (2010) following the method by Uchida *et al.* (2006). Their magnetic nucleus is composed of stoichiometric magnetite (Walls *et al.* 2013), but may be slightly maghemized due to storage in a refrigerator. TEM analysis (Fig. 1) shows some clustering, suggesting the likely presence of some magnetostatic interactions, and a narrow grain-size distribution of nearly equant particles. An analysis of the dimensions of the grains in TEM images showed a median diameter of 8.8 nm, with 90 per cent of the grains being between 6.2 and 11.6 nm (Fig. 2a) and a median aspect ratio (obtained from two-dimensional images) of 1.14 with 90 per cent of the grains having an aspect ratio between 1.01 and 1.38 (Fig. 2b), and the image shows some clustering of the magnetic grains. In contrast a Wohlfarth–Cisowski test (Wohlfarth 1958; Cisowski 1981) at 10 K has an IRM acquisition and

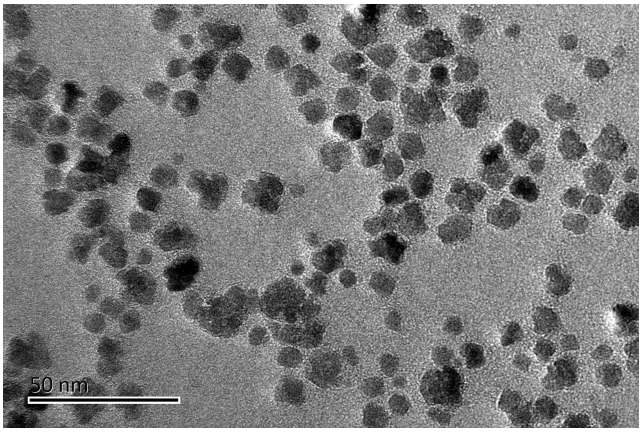

Figure 1. Transmission electron microscopic image of the magnetoferritin sample.

back-field demagnetization cross over value of 0.45, which indicates minor interactions. The back-field curves indicate a coercivity of remanence of $H_{cr} = 20$ mT. Hysteresis loops show that the sample saturates around ∼200 mT at 10 K and is superparamagnetic (SP) at room temperature (Fig. 3b). The hysteresis parameters were $M_{rs} = 0.087$ Am^2, $M_s = 0.34$ Am^2, $H_c = 15$ mT, leading to the ratios $M_{rs}/M_s = 0.26$ and $H_{cr}/H_c = 1.30$ which suggest dominant uniaxial single-domain behaviour (Day *et al.* 1977). A field cooling (FC) curve shows that all remanence is lost at ∼150 K, while a zero-field cooling curve confirms that no grains acquire a remanence at room temperature (Fig. 3c). Additionally, a thermal demagnetization curve of a saturating isothermal remanent magnetization (Fig. 3c) is similar to the FC curve and reveals that most unblocking occurs at low temperatures below ∼50 K and no remanence remains above ∼150 K. Frequency-dependent susceptibility curves show a broad peak around ∼200 K (Fig. 3d), and the out-of-phase curve drops to zero at 300 K, confirming the SP behaviour of the grains at room temperature.

5 EXPERIMENTAL METHODS

This study aims to experimentally test the two relationships given by eqs (24) and (26): the first is needed to relate the heating rate r of a CTD experiment to the effective time t_{eff}, and the second is used to create Pullaiah-style nomograms. Together they can be used to interpret CTD data to obtain, for example, acquisition times or temperatures of magnetic remanences, or cooling rates of rock bodies.

This was done by inducing a VRM of known acquisition time and temperature in the laboratory and then thermally demagnetizing it using CTD to determine the demagnetization (unblocking) temperature. The demagnetization time t_D is then calculated from eq. (26) and compared to the effective time calculated from the heating rate by eq. (24): comparing the two allows us to experimentally test eq. (24). Additionally, for calibration purposes described below, partial TRMs (pTRM) were acquired during cooling at known cooling rates in a second set of experiments, and then thermally demagnetized, thus comparing acquisition at a known cooling rate to demagnetization at a known heating rate. Experiments were carried out on Magnetic Properties Measurement Systems (MPMS) at the IRM (Superconducting quantum interference device MPMS2) and at IGGCAS (MPMS XL).

5.1 Method for VRMs: acquisition at constant temperature, demagnetization by continuous heating

The validity of eq. (24) (under the assumption that eq. (26) holds) was experimentally tested, that is,

$$\frac{T_A \ln(2t_A/\tau_0)}{1-(T_A/T_C)} = \frac{T_D \ln(2t_{\text{eff}}(r_D)/\tau_0)}{1-(T_D/T_C)}, \tag{27}$$

where the notation $t_{\text{eff}}(r)$ has been adopted to describe the effective time as a function of heating rate, according to eq. (24). A VRM of known acquisition time t_A and temperature T_A is compared to the demagnetization temperature T_D and heating rate r_D of a continuous heating thermal demagnetization experiment. The experimental procedure was:

(1) The sample was cooled to the acquisition temperature T_A in zero field.

(2) Once the temperature was stabilized, a magnetic field H_0 of 1 mT was applied and held for a time t_A between 1000 s and 16 000 s.

(3) The field was switched off and the sample was immediately heated in zero field at a set heating rate r_D between 0.25 and 5 K min^{-1}, while continuously measuring its remanent magnetization.

(4) Once the sample reached room temperature, it was alternating-field (AF) demagnetized to erase any remaining remanence.

The process was then repeated at various different acquisition times and temperatures, and different heating rates. The 1 mT field

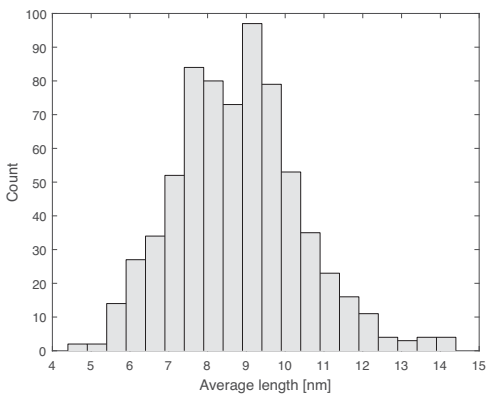

(a) Histogram of average diameter.

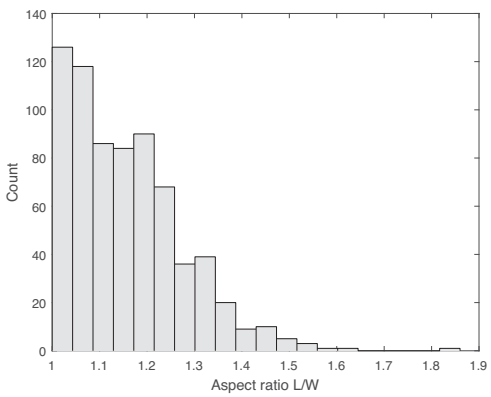

(b) Histogram of aspect ratios.

Figure 2. Histograms of the grain size distribution of the magnetoferritin sample determined by TEM.

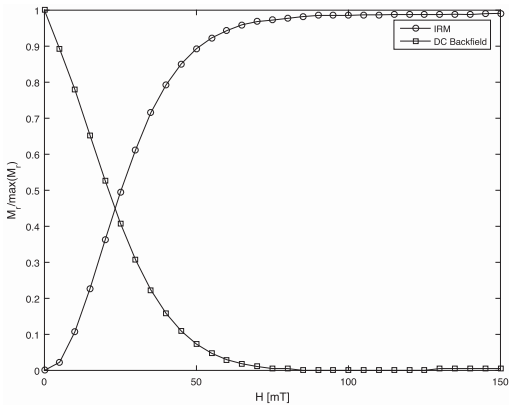

(a) IRM acquisition and back-field demagnetization curves at 10 K.

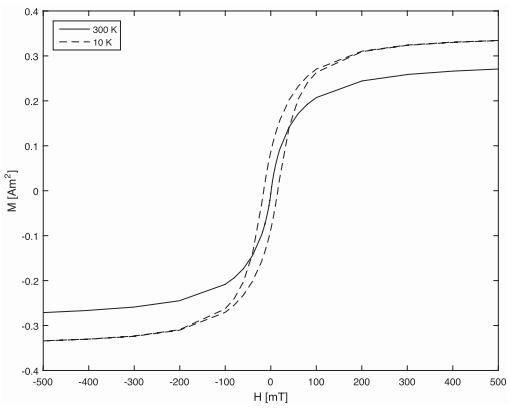

(b) Hysteresis loops at 10 K and at room temperature.

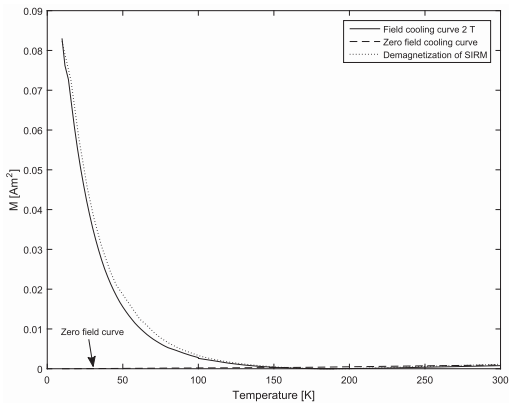

(c) Field cooling (FC) curve acquired in a 2 T field, zero-field cooling (ZFC) curve, and thermal demagnetization curve of a saturating isothermal remanent magnetization (SIRM) acquired at 10 K.

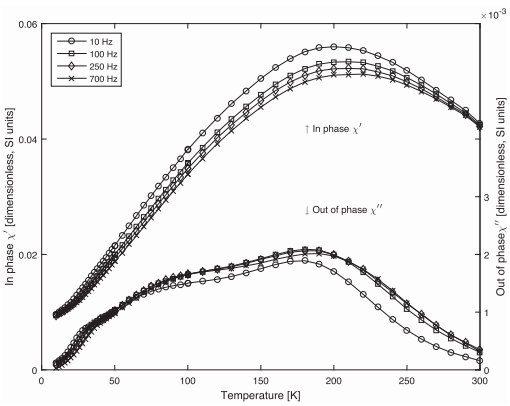

(d) Frequency-dependent susceptibility curves.

Figure 3. Rock magnetic characterization of the magnetoferritin sample.

was chosen because it is a reasonable low field that still allowed a good field control on the MPMS.

5.2 Method for pTRMs: acquisition by continuous cooling, demagnetization by continuous heating

Another set of experiments were performed to test eq. (26),

$$\frac{T_A \ln\left(2t_{\text{eff}}\left(r_A\right)/\tau_0\right)}{1-\left(T_A/T_C\right)} = \frac{T_D \ln\left(2t_{\text{eff}}\left(r_D\right)/\tau_0\right)}{1-\left(T_D/T_C\right)}, \tag{28}$$

where the left-hand side refers to remanence acquisition on cooling at rate r_A and the right-hand side to demagnetization of the same set of grains on heating at rate r_D. This experiment serves two important calibration purposes that will become clear in the following sections: first, determining the demagnetization temperature from the magnetic moment measurements $M_r(T)$ (a function that can in principle have any shape) is difficult and must be calibrated, and second, an important rock magnetic property, the atomic attempt time τ_0 (which appears in 26) is needed to plot Pullaiah nomograms, and must be determined—the data of this experiment can be used for this purpose as shown below.

The experimental procedure was:

(1) The MPMS was set to cool the sample at a set cooling rate r_A (between 0.25 and 8 K min^{-1}) to a target temperature of T_0, in zero field.

(2) During this process, as soon as the sample swept through a predefined acquisition temperature T_A, a 1 mT field was switched on, without interrupting the cooling process.

(3) Once the temperature had reached T_0, the field was switched off and the sample was heated in zero field at a set heating rate r_D between 0.25 and 5 K min^{-1}, while continuously measuring its remanent magnetization.

(4) Once the sample reached room temperature, it was AF demagnetized to erase any remaining remanence.

The process was then repeated at various different cooling and heating rates and acquisition temperatures. While the previous procedure creates VRMs and demagnetizes them, this procedure creates pTRMs and demagnetizes them thermally.

5.3 Determination of the demagnetization temperature T_D

Typically, the demagnetization temperature is determined by choosing the temperature where the remanent magnetization $M_r(T)$ drops

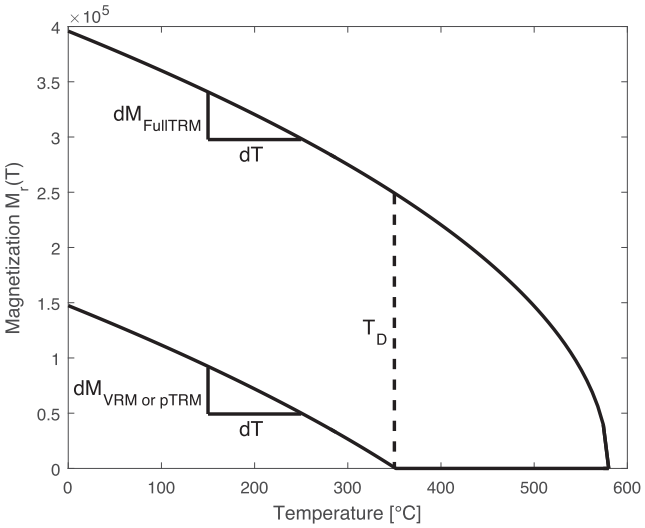

Figure 4. Schematic drawing of the remanent magnetization during thermal demagnetization experiments of a full TRM and of a partial TRM or VRM. Note that the shape of the curves depend on both the shape of $M_s(T)$ and on the grain size distribution.

to zero. In practice, however, the magnetic moment rarely drops to exactly zero because of instrumental noise. Moreover, the shape of the demagnetization curve $M_r(T)$ will depend strongly on the grain size/coercivity spectrum of the grains (with blocking temperatures below T_A) present, such that the remanence just a few degrees below the demagnetization temperature could be very small compared to the initial remanence. As the demagnetization temperature has to be determined accurately for this type of study, an objective criterion is needed to determine T_D. In this treatment, it is important to understand what is meant be acquisition and demagnetization temperatures, as opposed to blocking and unblocking temperatures: the acquisition temperature is the temperature to which a sample was heated in field. This process magnetizes all grains with blocking temperatures below and up to the acquisition temperature. The demagnetization temperature is the temperature a sample is heated in zero-field (in a CTD experiment) and demagnetizes all grains with unblocking temperatures below and up to the demagnetization temperature. The aim of eqs (27) and (28) is to find the demagnetization temperature that is necessary to demagnetize the same grains that previously acquired a remanence at the given acquisition temperature.

The procedure illustrated in Fig. 4 has been adopted that removes the dependence of the blocking/coercivity spectrum: First, a full TRM was created by cooling a sample in a 1 mT field from room temperature to the minimum temperature used in the experiment s described above. This full TRM was then demagnetized by CTD and measured, $M_{\mathrm{FullTRM}}(T)$. Afterwards, the experiments described in Sections 5.1 and 5.2 were carried out, yielding various thermal demagnetization curves, $M_{\mathrm{VRM}}(T)$ or $M_{p\mathrm{TRM}}(T)$, respectively; for each curve the acquisition temperature and time or cooling rate, respectively, were known. Below the blocking temperature, the shape of the demagnetization curves of the pTRMs and VRMs, is roughly the same as $M_{\mathrm{FullTRM}}(T)$, as all the grains should have been magnetized. Therefore, dividing the derivative of the demagnetization curve of the VRM or pTRM by the derivative of the full TRM,

$$\hat{M} = \frac{\mathrm{d}M_{\mathrm{VRM\,or\,pTRM}}/\mathrm{d}T}{\mathrm{d}M_{\mathrm{FullTRM}}/\mathrm{d}T}\,, \tag{29}$$

should be close to one below the demagnetization temperature. However, above the demagnetization temperature the differential of the VRM or pTRM should be close to zero, while the differential of the full TRM should still be large; the derivative should sharply drop from one to zero at the demagnetization temperature. More mathematically,

$$M_{\mathrm{FullTRM}} = \int M_s V f(V)\, n_{\mathrm{FullTRM}}(V)\, \mathrm{d}V\,, \tag{30}$$

and

$$M_{p\mathrm{TRM\,or\,VRM}} = \int M_s V f(V)\, n_{\mathrm{pTRM\,or\,VRM}}(V)\, \mathrm{d}V\,, \tag{31}$$

and therefore

$$\hat{M} = \frac{\mathrm{d}M_{\mathrm{pTRM\,or\,VRM}}}{\mathrm{d}M_{\mathrm{FullTRM}}} = \frac{n_{\mathrm{pTRM\,or\,VRM}}}{n_{\mathrm{FullTRM}}}\,, \tag{32}$$

where $\hat{M}$ does not depend on the grain size distribution, but only on the equilibrium magnetization at the respective blocking volume/temperature.

5.4 Field correction

Eq. (3) is valid for weak fields; for stronger fields above ∼300 μT, eq. (2) is applicable (Dunlop & Özdemir 1997). As the acquisition field is $H_0 = 1$ mT, eqs (27) and (28) must be modified using eq. (2), giving

$$\frac{T_A \ln(t_A/\tau_0)}{1-(T_A/T_C)}\left(1-\frac{|H_0|}{H_K}\right)^{-2} = \frac{T_D \ln(2t_{\mathrm{eff}}(r_D)/\tau_0)}{1-(T_D/T_C)}\,, \tag{33}$$

and

$$\frac{T_A \ln(t_{\mathrm{eff}}(r_A, H_0)/\tau_0)}{1-(T_A/T_C)}\left(1-\frac{|H_0|}{H_K}\right)^{-2} = \frac{T_D \ln(2t_{\mathrm{eff}}(r_D)/\tau_0)}{1-(T_D/T_C)}\,. \tag{34}$$

For convenience, and in order to be able to plot both kinds of data on a single plot, we define a field-corrected (effective) acquisition time,

$$t'_A = \frac{t_A^{\eta}}{2\tau_0^{\eta-1}}\,, \tag{35}$$

and

$$t'_{\mathrm{eff}}(r_A, H_0) = \frac{t_{\mathrm{eff}}^{\eta}(r_A, H_0)}{2\tau_0^{\eta-1}}\,, \tag{36}$$

respectively, where

$$\eta = \left(1-\frac{H_0}{H_K}\right)^{-2}\,. \tag{37}$$

5.5 Calibration of demagnetization temperature determination

Before taking the derivatives of the demagnetization data it is necessary to smooth the data, which is done using a spline fit to both M_{FullTRM} and the $M_{\mathrm{pTRM\,or\,VRM}}$ curves. Theory predicts that $\hat{M}$ should be a step-function, however, in practice this is rarely the case, for the following reasons:

(1) Because the acquisition temperatures differ between the pTRMs/VRMs and the full TRM, the magnetic moment caused

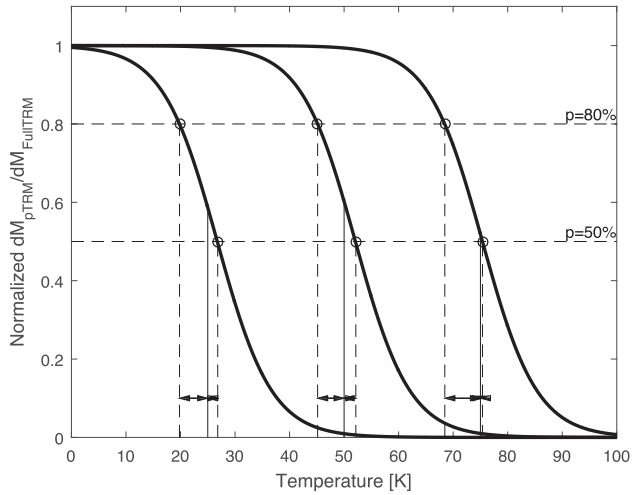

Figure 5. Schematic drawing of the $\tilde{M}$ curves (bold lines) for three pTRMs with expected demagnetization temperatures of 25, 50 and 75 K (solid lines, calculated from the known acquisition temperatures and cooling rates using eq. 34). Dashed lines show different choices of the parameter p used to determine the unblocking temperatures, together with the resulting demagnetization temperatures T_D. Ideally the mismatch (arrows) between the expected demagnetization temperature (solid lines) and measured demagnetization temperatures (dashed lines) should be zero for some choice of p.

by the same blocked grains will differ according to the different equilibrium states given by a Maxwell–Boltzmann distribution ($n_{\rm eq} = \tanh(VH_0M_s/kT)$, Néel 1949): lower acquisition temperatures T_A lead to a higher equilibrium magnetization $n_{eq}(T_A)$. Therefore the shape of the demagnetization curve differs slightly for the VRMs from the full TRMs.

(2) Various different heating rates are used for the demagnetization of the pTRMs/VRMs, but the $\hat{M}$ curves for all of them are calculated with by the same full TRM demagnetized at only one heating rate. The difference in heating rate will cause slight differences in the demagnetization curves.

(3) Although heating and cooling rates are set to constant values, the MPMS does have some deviation from the target rates. In particular, the first few minutes and the last few minutes have significant deviations, most notably for the highest and the lowest heating/cooling rates. On the MPMS at IGGCAS, there were also slight oscillations in the cooling rate.

(4) The field is supposed to be instantaneously switched on, but in practice it takes a finite time. In the pTRM experiments, this means that the field is ramping up while the temperature is decreasing at a given rate, smearing out the blocking temperature.

(5) The thermal demagnetization is assumed to be in zero field, however, there are typical residual fields in the MPMS of the order of μT.

(6) All of the samples had a non-zero magnetic moment at room temperature, which may be due to a remaining remanent magnetization and/or because of a residual field.

The remaining magnetic moment at room temperature was removed from the data by applying and subtracting a line fit over the highest temperature range and the $\hat{M}$ curves were normalized. The $\hat{M}$ curves then approximated step functions with a smooth decay from one towards zero over a finite temperature range. The 'measured demagnetization temperatures T_D' were chosen to be the temperatures where $\hat{M}$ decayed to p times its initial value (Fig. 5). The parameter p is chosen as a best-fit parameter that minimizes the mismatch between the 'measured demagnetization temperatures' and the 'expected demagnetization temperatures T_D' (i.e. those calculated from the known acquisition temperatures and rates using eq. 34). Ideally, for some choice of p, the mismatch between the two should be zero. One could minimize the sum of the squares of the misfits of the demagnetization temperatures (arrows in Fig. 5), but this would be inappropriate, as eq. (34) that is used to calculate the expected T_D, depends on the attempt time τ_0, which is unknown and has to be determined from the pTRM experiments (Section 5.6). For this reason, the p is chosen that minimizes total residual error of τ_0 (sum of the squares of the misfit in blocking volumes). The same p was then used for the VRM experiments.

5.6 Determination of the attempt time τ_0

The atomic attempt time τ_0 in eq. (28) strongly influences the shape of Pullaiah nomograms and it is therefore critically important for any study aiming to infer VRM/TRM acquisition times, temperatures or cooling rates, to determine it accurately. It also needs to be known for eq. (24), to calculate effective timescales so that CTD experiments can be interpreted. Literature values for the attempt time vary by orders-of-magnitude, however (see Berndt *et al.* 2015, and references therein). Fortunately, it can be determined from the pTRM data described in Section 5.2 using a least-squares algorithm : Either side of the equation is equal to the blocking volume, therefore the blocking volume V can be calculated from: (1) $t_{\rm eff}(r_A)$ and T_A and (2) from $t_{\rm eff}(r_D)$ and T_D. The difference ($\ln V_A - \ln V_D$) gives a measure of the deviation from the equation. The attempt time was chosen to be the value that minimizes the sum of the squares of ($\ln V_A - \ln V_D$) of all the data points (for various different heating and cooling rates, and acquisition temperatures).

6 RESULTS

Fig. 6 shows the magnetoferritin data of the raw demagnetization curves after smoothing. At low temperatures both the pTRM and the VRM curves follow the shape of the full TRM curve at low temperatures, although the first few measurements of the VRMs are likely to have experienced some thermal lag and show less decay than expected.

Despite the noise introduced by taking the derivatives the approximate step function shape is visible in the $\hat{M}$ curves (Fig. 7). For the magnetoferritin sample, most pTRM unblocking occurs over a range of ∼10 K, and for the VRMs over ∼5 K. The percentages p of the magnetization decay that yielded best fits for the demagnetization temperatures were strongly sample-dependent and lay between 54 per cent and 82 per cent, with values of the atomic attempt time being 9×10^{-10} s for the magnetoferritin, 1×10^{-13} s for 12-01 and 3×10^{-10} s for 12-07 (Table 1).

Fig. 8 relates the resulting demagnetization temperatures and times to the acquisition temperatures and times on a nomogram. The grey contour lines are calculated after Pullaiah *et al.* (1975) using the τ_0 value as determined for each sample. Sample 12-01 (Fig. 8b) is very noisy, which may explain the low value of τ_0 obtained. In all of the plots, there are various acquisition–demagnetization (solid diamonds and open circles, respectively) pairs with almost equal effective time $t_{\rm eff}$. These are data points for which the heating rate was set to be twice the cooling rate, such that, according to eq. (34), the field-corrected effective time is approximately equal. In these cases, the acquisition and demagnetization temperatures should be equal, which is true to about 1 K accuracy in most cases.

After p and τ_0 were obtained from the pTRM data, the VRM data were plotted on nomograms using the same p and τ_0 values

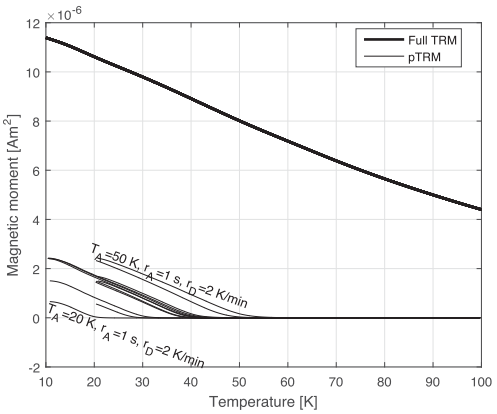

(a) pTRMs acquired on cooling at a rate r_A and applying a 1 mT field once the temperature sweeps through the acquisition temperature T_A.

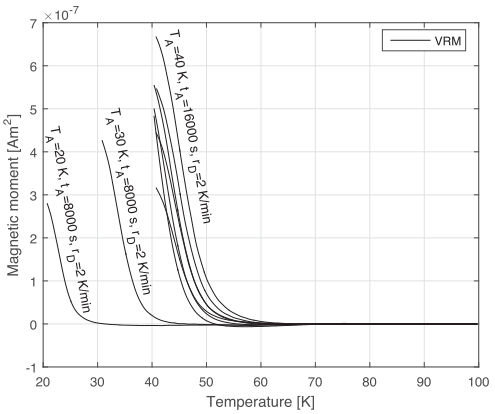

(b) VRMs acquired at constant acquisition temperatures T_A of 20, 30 and 40 K, over different acquisition times t_A (Full TRM is not shown, as it is about an order of magnitude stronger than VRMs).

Figure 6. Magnetic moment on continuous thermal demagnetization at different heating rates r_D of the magnetoferritin sample MFn1 for VRMs and pTRMs acquired at various different acquisition temperatures T_A, acquisition times t_A (VRMs) / cooling rates r_A (pTRMs). For clarity, only T_A, t_A, r_A and r_D are given only for some curves. Full TRM curves were acquired on cooling from 300 to 10 K.

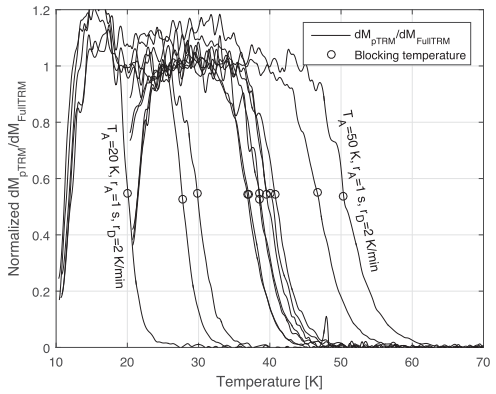

(a) $\hat{M}$ curves of pTRMs acquired on cooling at a rate r_A and applying a 1 mT field once the temperature sweeps through the acquisition temperature T_A.

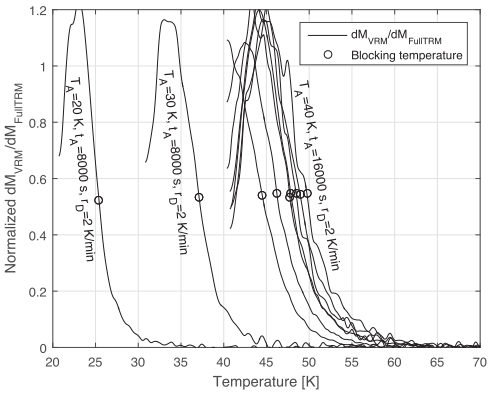

(b) $\hat{M}$ curves of VRMs acquired at constant acquisition temperatures T_A of 20, 30 and 40 K, over different acquisition times t_A.

Figure 7. $\hat{M}$ curves on continuous thermal demagnetization at different heating rates r_D of the magnetoferritin sample MFn according to eq. (29) for VRMs and pTRMs acquired at various different acquisition temperatures T_A, acquisition times t_A (VRMs) / cooling rates r_A (pTRMs). For clarity, only T_A, t_A, r_A and r_D are given only for some curves. Circles indicate blocking temperatures as determined by the method described in Section 5.5.

Table 1. Summary of best-fit values.

Sample	p	τ_0 (s)
Magnetoferritin	54 per cent	9×10^{-10}
TC04-12-01	82 per cent	1×10^{-13}
TC04-12-07	70 per cent	3×10^{-10}

(Fig. 9). For most combinations of T_A and t_A (solid diamonds), three to four different heating rates (open circles) were used to obtain T_D and r_D. The figures show that the open circles (T_D and r_D) generally fall onto straight lines with a slope that tends to be slightly lower than the nomograms. The lines connecting the acquisition times/temperatures to the demagnetization times/temperatures tend to be slightly steeper than predicted by the nomograms. This means that, compared to eq. (24): (1) longer demagnetization times are offset downwards, while (2) shorter demagnetization times are offset upwards; the effective time should therefore have a stronger heating rate r_D dependence than predicted by theory. Moreover, the mismatch seems to be more pronounced in sample 12-07 (Fig. 8c), particularly at higher temperatures. This suggests that eq. (24) should also have a stronger temperature dependence than predicted. As these deviations are not observed in the pTRM experiments, they cannot be explained by thermal lag on heating.

To quantify the deviation from theory, the effective times calculated from eq. (24) are plotted against the expected demagnetization time t_D calculated from eq. (26) for all the samples in Fig. 10(a). If eq. (24) is correct, then all points should fall onto the diagonal ($t_{\rm eff} = t_D$, dashed line). However, it is observed that while there is a strong linear correlation between the two on a log-log scale, the slope deviates significantly. A linear least-squares regression yields a slope of 0.54 ± 0.03 with a y-offset of 2.66 ± 0.10. It is also observed that in the central area of the plot (10–100 s), the data points of sample 12-07 that had the highest blocking temperatures consistently lie below the regression line, whereas the data points of the other two samples that had lower blocking temperatures fall above. Moreover, for each of the individual samples, the slope of a regression line would be slightly steeper than for the whole data set. As the temperature range for each sample was rather limited (a few

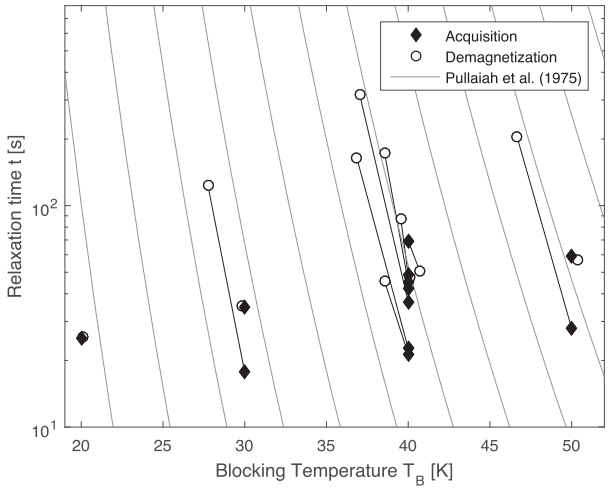

(a) Magnetoferritin.

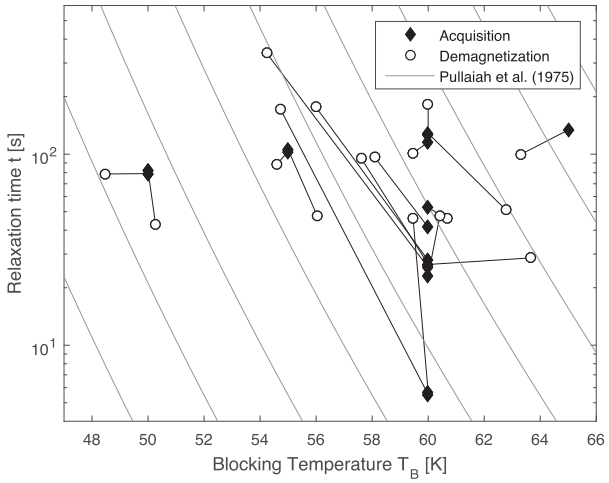

(b) Tiva Canyon 12-01.

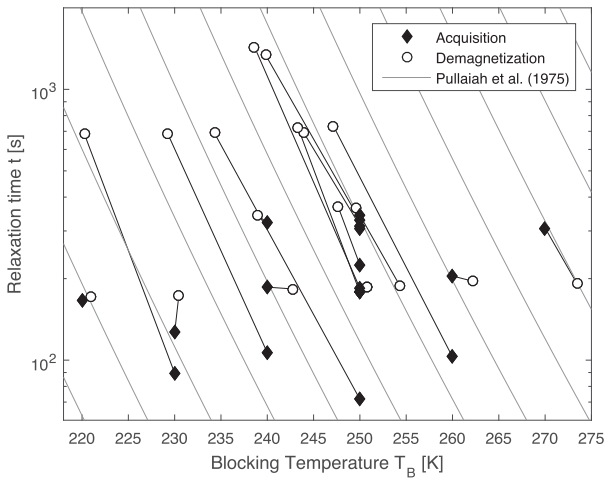

(c) Tiva Canyon 12-07.

Figure 8. Nomograms of pTRMs acquired at T_A and t_A given by solid diamonds and demagnetized at T_D and t_D given by open circles, where the effective times t_A and t_D are obtained from cooling rates r_A and heating rates r_D by eq. (24). Pullaiah *et al.* (1975) nomograms (eq. 26) are indicated for the τ_0 that best fits the experimental data.

tens of degrees), while the heating rate range was large (orders of magnitude), this variation within one sample can likely be attributed to the heating rate, while the variation between sample 12-07 and the other two can likely be attributed to the temperature difference.

From eq. (25), we find that on a logarithmic scale

$$\ln t_{\text{eff}} = c_1 \ln\left(\frac{T}{T_C}\right) + c_2 \ln\left(\frac{c_3}{r}\right) + \ln\left[(T_C - T)/\ln\left(\frac{2T}{r\tau_0}\left(1 - \frac{T}{T_C}\right)\right)\right], \quad (38)$$

where $c_1 = c_2 = c_3 = 1$, the value of $\ln t_{\text{eff}}$ is dominated by the first two terms, with the third term being a relatively constant term at temperatures significantly below the Curie temperature. On logarithmic scales, t_{eff} should approximately be a plane in r– T/T_C-space with the slopes along both axes equal to one (Fig. 11). A least-squares regression plane yields the slopes $c_1 = 1.87 \pm 0.10$, $c_2 = 1.48 \pm 0.10$ and $c_3 = 0.53 \pm 0.09\,\text{Ks}^{-1}$. This suggests that eq. (25) should be modified with a correction factor

$$t'_{\text{eff}} = \frac{\tau_0}{2} \exp\left\{W\left(\frac{2}{\tau_0}\left(\frac{T}{T_C}\right)^{c_1}\left(\frac{c_3}{r}\right)^{c_2}(T_C - T)\right)\right\}, \quad (39)$$

that amplifies the temperature and heating rate dependence of the effective time.

The nomograms are redrawn using the corrected t'_{eff} and compared to the uncorrected t_{eff} nomograms (Fig. 9) where the improvement in agreement of the data with the nomograms can be clearly seen. To quantify the improvement, the sum of squares of the differences in theoretic al and empirical blocking volumes ($\ln V_A - \ln V_D$) as described in Section 5.6 is calculated. The total errors show a substantial improvement from the uncorrected to the corrected nomograms for all samples: from 1.14×10^{-3} to 4.58×10^{-4} for the magnetoferritin, from 1.16×10^{-3} to 1.71×10^{-4} for sample 12-01 and from 5.34×10^{-4} to 3.47×10^{-4} for sample 12-07 (Table 2).

7 DISCUSSION

This study has shown that eq. (24), which follows from Néel (1949) theory, should theoretically make it possible to use standard Pullaiah nomograms to relate demagnetization temperatures from CTD experiments to acquisition times, temperatures or cooling rates. However, the equation does not accurately predict our experimental observations: Empirically, the relation was modified incorporating coefficients that amplify both the temperature and the heating rate dependence of the effective time. After the correction Pullaiah nomograms accurately relate acquisition and demagnetization times/temperatures/rates. This result has two important implications: First, it can help establish CTD as a mainstream palaeomagnetic method, as it helps to interpret blocking temperatures from them, which was previously not possible. Second, it is likely that the converse also holds true, that is, an empirical correction is also needed to relate stepwise thermal demagnetization data to cooling rates of slowly cooling rock bodies – a fact that is important for the geological interpretation of such bodies.

The correction was needed for all three studied samples and reduces the effective time by up to one order-of-magnitude. Physically, the modification of the effective time means that continuous heating is less effective at removing a magnetization than stepwise heating: higher temperatures (or longer times, i.e. slower heating rates) than predicted from eq. (26) and (24) are needed to remove a magnetization. This would be the case, if higher temperatures have a relatively stronger demagnetizing effect compared to lower temperatures, than predicted by Néel (1949) theory: stepwise thermal

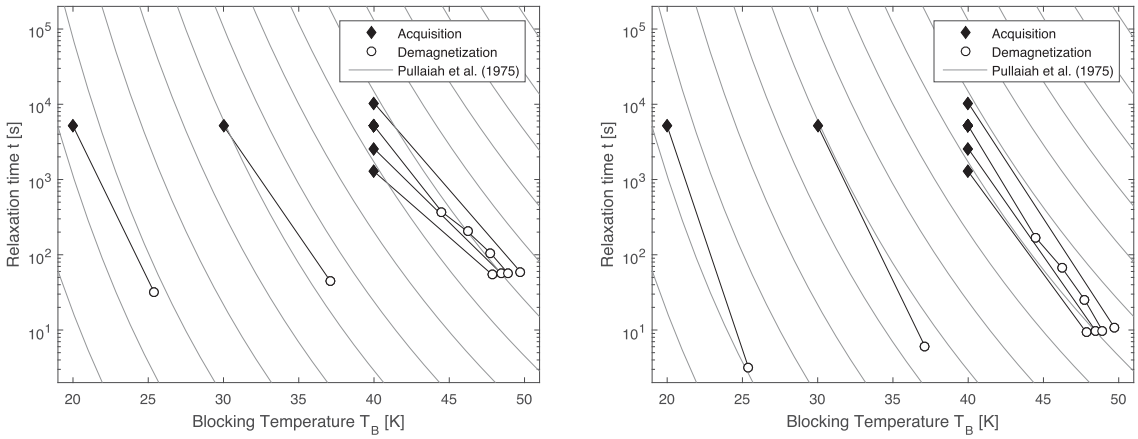

(a) Magnetoferritin, uncorrected. (b) Magnetoferritin, corrected.

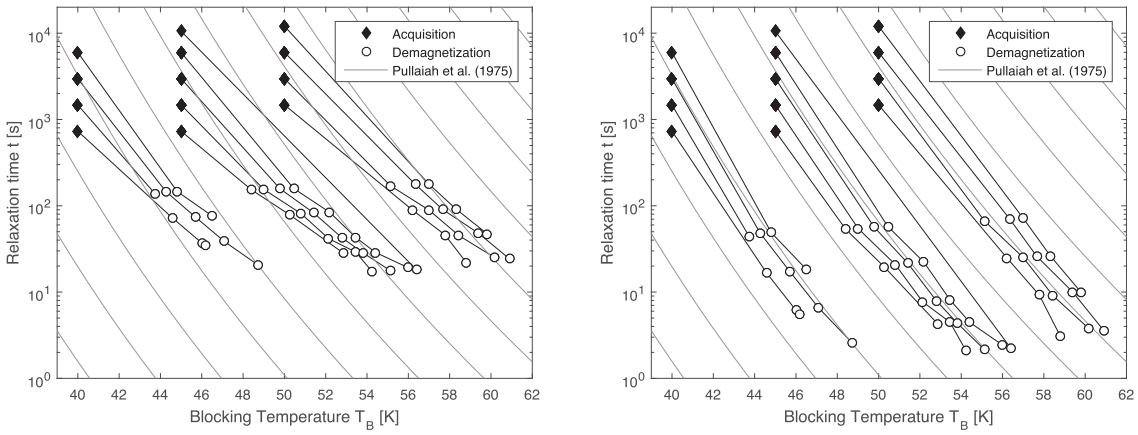

(c) 12-01, uncorrected. (d) 12-01, corrected.

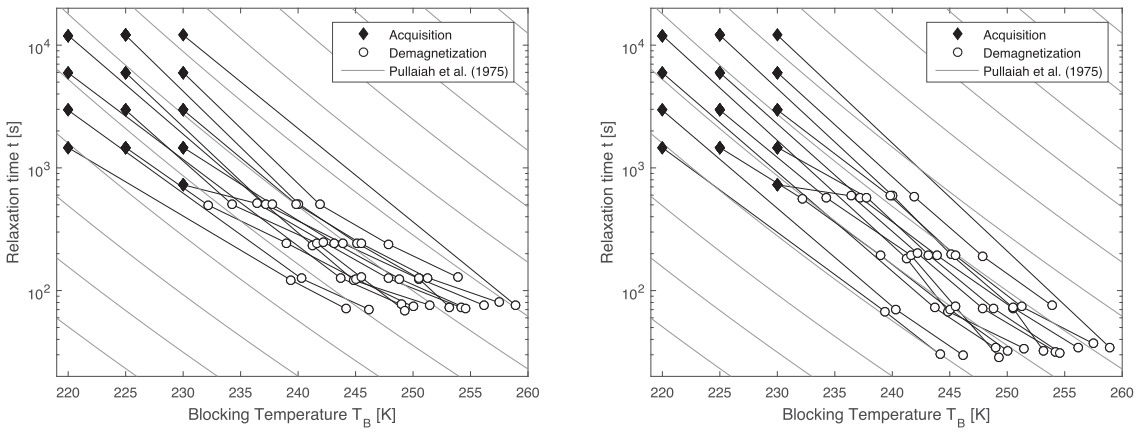

(e) 12-07, uncorrected. (f) 12-07, corrected.

Figure 9. Nomograms of VRMs acquired at T_A and t_A given by solid diamonds and demagnetized at T_D and t_D given by open circles, where the effective times t_D are obtained from the heating rates r_D by eq. (24). Pullaiah *et al.* (1975) nomograms (eq. 26) are indicated for the τ_0 that best fits the experimental pTRM data shown in Fig. 8.

demagnetization keeps the highest temperature step for a prolonged time, whereas the highest temperature in CTD is a transient state (i.e. instantaneous). This may be the case for PSD grains, where the energy barriers to rotate a vortex structure are a function of temperature (Muxworthy *et al.* 2003; Almeida *et al.* 2016). However, only one sample (12-07) is likely to contain some PSD grains, and the magnetoferritin sample, which contained only SD grains (SP at room temperature), also required the correction. Magnetostatic interactions are weak in the samples, but may be strong enough to have an impact, and may explain the discrepancy for the magnetoferritin sample. In a similar way to PSD grains, interactions may lead to higher energy barriers at lower temperatures and vice versa, making CTD less effective at demagnetization. A further effect may be magnetocrystalline anisotropy, in which case the

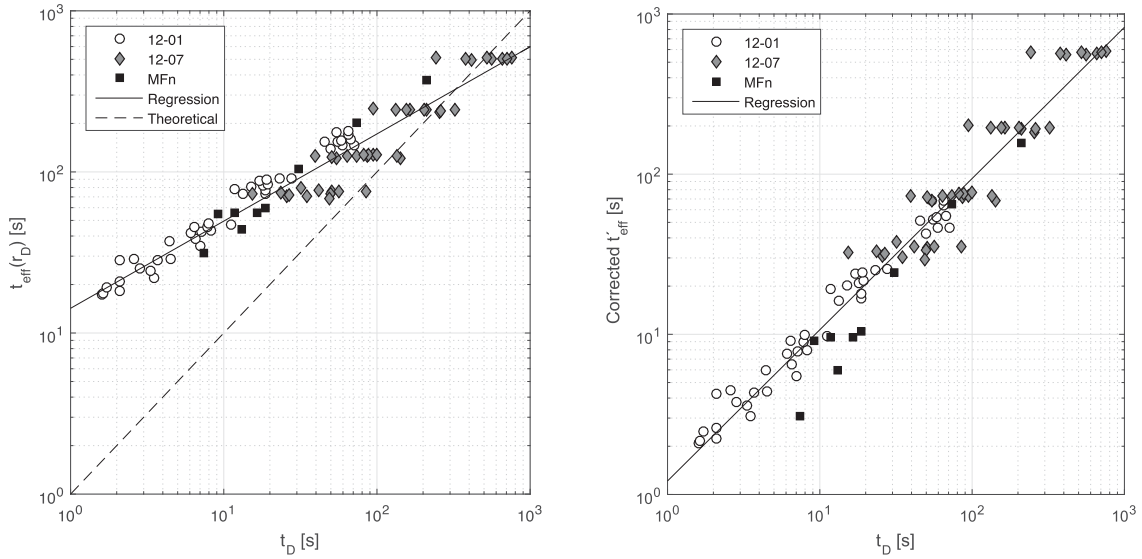

(a) Uncorrected. (b) Corrected according to eq. (39).

Figure 10. Plot of the quantity effective time $t_{\rm eff}(r_D)$ as calculated from calculated from eq. (24) versus the expected demagnetization time t_D as predicted from Néel (1949) theory from eq. (26), uncorrected and corrected. In theory, $t_{\rm eff}$ and t_D should be equal and the dots should fall onto the diagonal (dashed line in Fig. 10a).

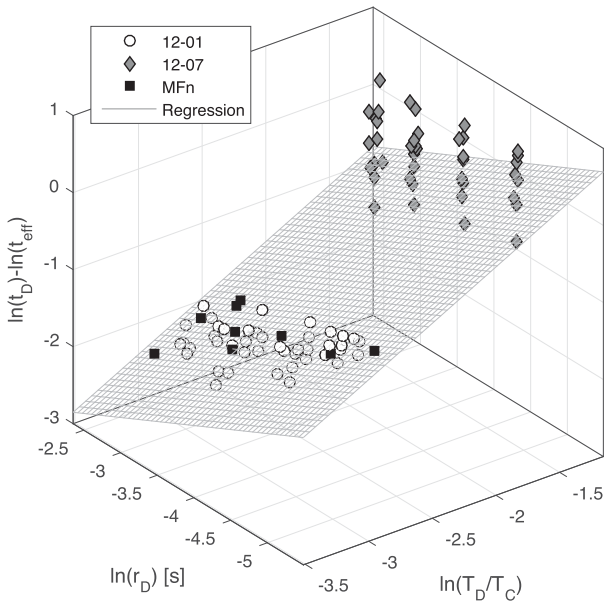

Figure 11. Regression to determine correction coefficients in eq. (39).

Table 2. Summary of the sum of squares of the differences in theoretical and empirical blocking volumes ($\ln V_A - \ln V_D$) calculated for the nomograms using the uncorrected effective time (eq. 24) and the corrected effective time (eq. 39).

Sample	Uncorrected $t_{\rm eff}$	Corrected $t'_{\rm eff}$
Magnetoferritin	1.14×10^{-3}	4.58×10^{-4}
12-01	1.16×10^{-3}	1.71×10^{-4}
12-07	5.34×10^{-4}	3.47×10^{-4}

temperature-dependence of $H_K(T)$ varies with the tenth power of $M_s(T)$, rather than being directly proportional (Callen & Callen 1966). This would lead to an effective time with the term in round brackets in eq. (24) raised to the fifth power. Although this explanation is compelling, because the magnetoferritin sample contains a large proportion of almost equant grains that may likely be dominated by magnetocrystalline anisotropy, and the Tiva Canyon samples contain titanium which increases the contribution of magnetocrystalline anisotropy relative to pure magnetite, the effect is weak. For the magnetoferritin sample, a recalculation using dominant magnetocrystalline anisotropy yields effective times less than 20 per cent shorter than using shape anisotropy (versus an order-of-magnitude mismatch to the Pullaiah nomograms). For the Tiva Canyon 12-07 sample on the other hand, magnetocrystalline anisotropy would over-correct the effective times, but this sample is least likely to have a significant magnetocrystalline anisotropy due to its large grain size, high elongation, high blocking temperatures and low titanium content.

In addition to this main result, a number of other important observations were made in this study. The first one is that blocking occurs over a temperature range of 5–40 K (Figs 7 and 12). Lower-temperature experiments had a narrower blocking range 5–10 K and the higher temperature experiments of sample 12-07 had a broader blocking range around 30 K. This means that the concept of a blocking temperature introduced by Néel (1949), due to the strong exponential temperature dependence of the relaxation time, holds only approximately in practice: This range is narrow enough to be approximated by a single blocking temperature for most geological applications, although some studies in fundamental rock magnetism require a higher precision. The phenomenon is well known from Néel (1949) theory and was previously observed in synthetic stoichiometric 37 nm diameter SD magnetite by Dunlop & Özdemir (1993) in stepwise thermal demagnetization experiments that showed gradual unblocking over ranges of 40–55 K at high temperatures of 556–687 K (283–414 °C), suggesting that blocking occurs more gradually at higher temperatures, as would be expected from eq. (19). This trend is confirmed by the data of this study with an almost linear trend as indicated by a regression line (slope 0.12) on the blocking range as a function of acquisition temperature (Fig. 12).

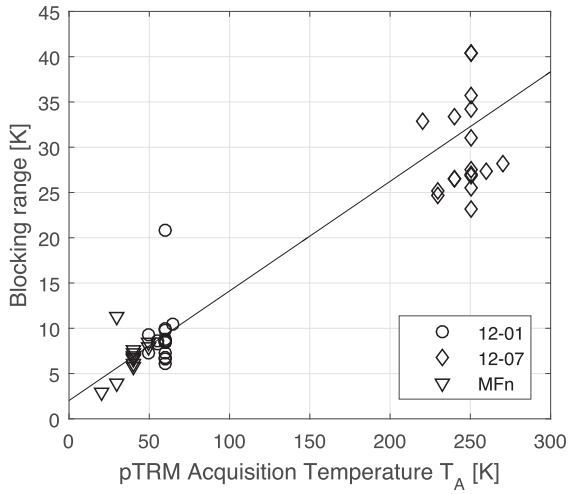

Figure 12. Temperature range were unblocking of $\hat{M}$ from 90 per cent to 10 per cent occurs (for TRM experiments), as a function of blocking temperature. Line indicates a linear regression and has slope 0.12.

The method presented here offers a way to empirically determine the percentage of magnetic decay corresponding to the blocking temperature from demagnetization data, but it has a strong sample dependence, ranging from 54 per cent to 82 per cent of the initial magnetization. No consistent trend of this value with neither temperature, grain-size nor domain state was found. PSD and MD grains are known to violate the simple relationship of blocking temperatures (eq. 26; Dunlop & Özdemir 2000), but only sample 12-07, which had an intermediate value of 70 per cent, is likely to contain PSD grains. Interacting SD and non-uniaxial SD grains also violate eq. (26) and may have played a role for the slightly interacting magnetoferritin sample. Dunlop & Özdemir (1993) found that for the 37 nm SD magnetite, the blocking temperature corresponded to a decay of 50 per cent of the initial magnetization, but their temperature resolution is relatively low (tens of degrees) due to the use of stepwise thermal demagnetization.

After determining the percentage to estimate blocking temperatures, eq. (26) (Néel 1949; Pullaiah *et al.* 1975) is shown to predict CTD blocking temperatures of pTRMs to ∼1 K (Fig. 8), which is within experimental uncertainties, if eq. (24) is used on both sides of eq. (26).

The pTRM experiments provided a method to determine τ_0; obtained values are 3×10^{-10} s for large grained (titano)magnetite (12-07), 1×10^{-13} s for small grained (titano)magnetite below the Verwey transition (12-01) and 9×10^{-10} s for magnetoferritin below the Verwey transition. The value for sample 12-01 is smaller than commonly assumed for (titano)magnetite, and smaller than previously determined by a recent method based on measuring temperature-dependent viscous decay (2×10^{-9} s for 12-07 and 4×10^{-10} s for 12-01, Berndt *et al.* 2015). It is likely that the τ_0 obtained for sample 12-01 is affected by the comparably large instrumental noise (Fig. 8b), but Berndt *et al.* (2015) also found that sample 12-01 had a smaller τ_0 than 12-07, suggesting the presence of one or more possible trends: (1) τ_0 may be larger for higher temperatures or larger SD grain-volumes (Berndt *et al.* 2015) as predicted by Néel (1949), (2) τ_0 may be smaller below the Verwey transition (although the Verwey transition tends to be suppressed in titanomagnetites), and (3) τ_0 may be larger in PSD grains. Although the two samples are mineralogically very similar, minor differences in mineralogy may also affect τ_0. The τ_0 obtained for the magnetoferritin is larger than previously determined for a similar magnetoferritin sample with smaller grain sizes ($\tau_0 = 1.1 \times 10^{-11}$ s, Cao *et al.* 2010), but in the range of commonly quoted values for magnetite.

8 CONCLUSIONS

Three main conclusions can be drawn from this study. First, eq. (24) derived from Néel (1949) theory, overestimates the effective demagnetization time of CTD experiments, or underestimates demagnetization temperatures. Empirically, the equation can be corrected to accurately predict effective times and demagnetization temperatures of all studied samples, but the physical reasons for the modification need to be further investigated. Second, the concept of a blocking temperature introduced by Néel (1949) holds only approximately in practice: depending on the temperature, blocking occurs gradually over an interval of 5–20 K. The predicted blocking temperature from Néel (1949) theory lies within this range, but does not generally correspond to 50 unblocking as observed by Dunlop & Özdemir (1993). Instead, the blocking temperature corresponds to a loss of p per cent of the magnetic moment, which is sample-dependent and can be determined experimentally. Third, the atomic attempt time τ_0 can be estimated by a best fit to Pullaiah nomograms. The nomograms predict blocking temperatures of pTRMs to a high accuracy (∼1 K). Compared to other methods to determine τ_0 (McNab *et al.* 1968; Dickson *et al.* 1993; Labarta *et al.* 1993; Iglesias *et al.* 1996; Moskowitz *et al.* 1997; Worm & Jackson 1999; Berndt *et al.* 2015) the one presented here is fast and easy, making use of only one instrument (MPMS), and being able to measure sufficient data for a τ_0 estimate in about a day.

ACKNOWLEDGEMENTS

This research was funded by a PhD placement grant by the British Research Council, NERC grant NE/J020508/1, and a visiting researcher fellowship by the Institute of Rock Magnetism (IRM) to TB. The IRM is a US National Multi-user Facility supported through the Instrumentation and Facilities program of the National Science Foundation, Earth Sciences Division, and by funding from the University of Minnesota. GAP acknowledges support from NSFC grants 41374072 and 41574063, and CAS project XDB18010203. We thank Yongxin Pan for his assistance. We are grateful to Karl Fabian for helpful discussions and advice.

REFERENCES

Almeida, T.P. *et al.*, 2016. Direct observation of the thermal demagnetization of magnetic vortex structures in nonideal magnetite recorders, *Geophys. Res. Lett.,* **43**(16), 8426–8434.

Berndt, T. & Muxworthy, A.R., 2017. Dating Icelandic glacial floods using a new viscous remanent magnetization protocol, *Geology,* **45**(4), 339–342.

Berndt, T., Muxworthy, A.R. & Paterson, G.A., 2015. Determining the magnetic attempt time τ_0, its temperature dependence, and the grain size distribution from magnetic viscosity measurements, *J. geophys. Res.,* **120,** 7322–7336.

Biggin, A.J., Badejo, S., Hodgson, E., Muxworthy, a.R., Shaw, J. & Dekkers, M.J., 2013. The effect of cooling rate on the intensity of thermoremanent magnetization (TRM) acquired by assemblages of pseudo-single domain, multidomain and interacting single-domain grains, *Geophys. J. Int.,* **193**(3), 1239–1249.

Cai, Y., Cao, C., He, X., Yang, C., Tian, L., Zhu, R. & Pan, Y., 2015. Enhanced magnetic resonance imaging and staining of cancer cells using ferrimagnetic H-ferritin nanoparticles with increasing core size, *Int. J. Nanomed.,* **10,** 2619–2634.

Callen, H.B. & Callen, E., 1966. The present status of the temperature dependence of magnetocrystalline anisotropy, and the l (l + 1)/2 power law, *J. Phys. Chem. Solids,* **27**(8), 1271–1285.

Cao, C., Tian, L., Liu, Q., Liu, W., Chen, G. & Pan, Y., 2010. Magnetic characterization of noninteracting, randomly oriented, nanometer-scale ferrimagnetic particles, *J. geophys. Res.,* **115,** B07103, doi:10.1029/2009JB006855.

Cao, C. *et al.*, 2014. Targeted in vivo imaging of microscopic tumors with ferritin-based nanoprobes across biological barriers, *Adv. Mater.,* **26**(16), 2566–2571.

Cisowski, S., 1981. Interacting vs. non-interacting single-domain behavior in natural and synthetic samples, *Phys. Earth planet. Inter.,* **26,** 56–62.

Creer, K., 1967. Thermal demagnetization by the continuous method, in *Methods in Palaeomagnetism: Proceedings of the NATO Advanced Study Institute on Palaeomagnetic Methods,* held in the Physics Department of the University of Newcastle Upon Tyne, April 1–10, 1964, vol. 3, p. 287.

Day, R., Fuller, M. & Schmidt, V.A., 1977. Hysteresis properties of titanomagnetites: grain-size and compositional dependence, *Phys. Earth planet. Inter.,* **13**(4), 260–267.

Dickson, D., Reid, N. & Hunt, C., 1993. Determination of f0 for fine magnetic particles, *J. Magn. Magn. Mater.,* **125,** 345–350.

Dodson, M., 1976. Kinetic processes and thermal history of slowly cooling solids, *Nature,* **259,** 551–553.

Dodson, M.H. & McClelland-Brown, E., 1980. Magnetic blocking temperatures of single-domain grains during slow cooling, *J. geophys. Res.,* **85,** 2625–2637.

Dunlop, D., 1983. Viscous magnetization of 0.04–100 μm magnetites, *Geophys. J. Int.,* **74,** 667–687.

Dunlop, D. & Özdemir, Ö., 1993. Thermal demagnetization of VRM and pTRM of single domain magnetite: no evidence for anomalously high unblocking temperatures, *Geophys. Res. Lett.,* **20**(18), 1939–1942.

Dunlop, D.J., 2009. Continuous and stepwise thermal demagnetization: are they equivalent?, *Geophys. J. Int.,* **177**(3), 949–957.

Dunlop, D.J. & Özdemir, Ö., 1997. *Rock Magnetism: Fundamentals and Frontiers,* Cambridge Univ. Press.

Dunlop, D.J. & Özdemir, Ö., 2000. Effect of grain size and domain state on thermal demagnetization tails, *Geophys. Res. Lett.,* **27**(9), 1311–1314.

Egli, R., 2002. Anhysteretic remanent magnetization of fine magnetic particles, *J. geophys. Res.,* **107,** EPM 2-1–EPM 2-21.

Enkin, R. & Dunlop, D., 1988. The demagnetization temperature necessary to remove viscous remanent magnetization, *Geophys. Res. Lett.,* **15**(5), 514–517.

Ferk, A., Aulock, F.W.V., Leonhardt, R., Hess, K.-U. & Dingwell, D.B., 2010. A cooling rate bias in paleointensity determination from volcanic glass: an experimental demonstration, *J. geophys. Res.,* **115,** B08102, doi:10.1029/2009JB006964.

Fox, J. & Aitken, M., 1980. Cooling-rate dependence of thermoremanent magnetisation, *Nature,* **283,** 462–463.

Halgedahl, S., Day, R. & Fuller, M., 1980. The effect of cooling rate on the intensity of weak-field TRM in single-domain magnetite, *J. geophys. Res.,* **85**(80), 3690–3698.

Iglesias, O., Badia, F., Labarta, A. & Balcells, L., 1996. Energy barrier distributions in magnetic systems from the T ln (t/τ_0) scaling, *Z. Phys. B,* **100**(2), 173–178.

Jackson, M. & Worm, H.-U., 2001. Anomalous unblocking temperatures, viscosity and frequency-dependent susceptibility in the chemically-remagnetized Trenton limestone, *Phys. Earth planet. Inter.,* **126**(1), 27–42.

Jackson, M., Carter-Stiglitz, B., Egli, R. & Solheid, P., 2006. Characterizing the superparamagnetic grain distribution $f(V, H_k)$ by thermal fluctuation tomography, *J. geophys. Res.,* **111,** B12S07, doi:10.1029/2006JB004514.

Kent, D., 1985. Thermoviscous remagnetization in some Appalachian limestones, *Geophys. Res. Lett.,* **12**(12), 3–6.

Kent, D. & Miller, J., 1987. Redbeds and thermoviscous magnetization theory, *Geophys. Res. Lett.,* **14**(4), 327–330.

Labarta, A., Iglesias, O., Balcells, L. & Badia, F., 1993. Magnetic relaxation in small-particle systems: ln (t/τ_0) scaling, *Phys. Rev. B,* **48**(14), 10 240–10 246.

Le Goff, M. & Gallet, Y., 2004. A new three-axis vibrating sample magnetometer for continuous high-temperature magnetization measurements: applications to paleo- and archeo-intensity determinations, *Earth planet. Sci. Lett.,* **229,** 31–43.

McClelland-Brown, E., 1984. Experiments on TRM intensity dependence on cooling rate, *Geophys. Res. Lett.,* **11**(3), 205–208.

McNab, T.K., Fox, R.A. & Boyle, A.J.F., 1968. Some Magnetic Properties of Magnetite (Fe_3O_4) Microcrystals, *J. Appl. Phys.,* **39**(12), 5703–5711.

Moskowitz, B.M., Frankel, R.B., Walton, S.A., Dickson, D.P., Wong, K., Douglas, T. & Mann, S., 1997. Determination of the preexponential frequency factor for superparamagnetic maghemite particles in magnetoferritin, *J. geophys. Res.,* **102**(97), 671–680.

Muxworthy, A.R., Williams, W. & Virdee, D., 2003. Effect of magnetostatic interactions on the hysteresis parameters of single-domain and psuedo-single domain grains, *J. geophys. Res.,* **108**(11), 1–13.

Muxworthy, A.R. & Heslop, D., 2011. A Preisach method for estimating absolute paleofield intensity under the constraint of using only isothermal measurements: 1. Theoretical framework, *J. geophys. Res.,* **116,** B04102, doi:10.1029/2010JB007843.

Muxworthy, A.R., Heslop, D., Paterson, G.A. & Michalk, D., 2011. A Preisach method for estimating absolute paleofield intensity under the constraint of using only isothermal measurements: 2. Experimental testing, *J. geophys. Res.,* **116,** B04103, doi:10.1029/2010JB007844.

Muxworthy, A.R., Evans, M.E., Scourfield, S.J. & King, J.G., 2013. Paleointensity results from the late-Archaean Modipe Gabbro of Botswana, *Geochem. Geophys. Geosyst.,* **14**(7), 2198–2205.

Muxworthy, A.R., Williams, J. & Heslop, D., 2015. Testing the use of viscous remanent magnetisation to date flood events, *Frontiers Earth Sci.,* **3,** 1–9.

Néel, L., 1949. Theory of magnetic viscosity of fine grained ferromagnetics with application to baked clays, *Ann. Geophys.,* **5,** 99–136.

Paterson, G.A., Roberts, A.P., Mac Niocaill, C. Muxworthy A.R., Gurioli, L., Viramonté, J.G., Navarro, C. & Weider, S., 2010. Paleomagnetic determination of emplacement temperatures of pyroclastic deposits: an under-utilized tool, *Bull. Volcanol.,* **72**(3), 309–330.

Pullaiah, G., Irving, E., Buchan, K. & Dunlop, D., 1975. Magnetization changes caused by burial and uplift, *Earth planet. Sci. Lett.,* **28,** 133–143.

Rosenbaum, J.G., 1993. Magnetic grain-size variations through an ash flow sheet: Influence on magnetic properties and implications for cooling history, *J. geophys. Res.,* **98**(93), 11 715–11 727.

Schlinger, C.M., Rosenbaum, J.G. & Veblen, D.R., 1988. Fe-oxide microcrystals in welded tuff from southern Nevada: origin of remanence carriers by precipitation in volcanic glass, *Geology,* **16,** 556–559.

Schlinger, C.M., Veblen, D.R. & Rosenbaum, J.G., 1991. Magnetism and magnetic mineralogy of ash flow tuffs from Yucca Mountain, Nevada, *J. geophys. Res.,* **96,** 6035–6052.

Schmidt, P. & Clark, D., 1985. Step-wise and continuous thermal demagnetization and theories of thermoremanence, *Geophys. J. R. astr. Soc.,* **83,** 731–751.

Shcherbakov, V.P. & Fabian, K., 2005. On the determination of magnetic grain-size distributions of superparamagnetic particle ensembles using the frequency dependence of susceptibility at different temperatures, *Geophys. J. Int.,* **162,** 736–746.

Thellier, E. & Thellier, O., 1959. Sur l'intensité du champ magnétique terrestre dans le passe historique et géologique, *Ann. Géophys.,* **15,** 285–376.

Till, J.L., Jackson, M.J., Rosenbaum, J.G. & Solheid, P., 2011. Magnetic properties in an ash flow tuff with continuous grain size variation: a natural reference for magnetic particle granulometry, *Geochem. Geophys. Geosyst.,* **12**(7), 1–10.

Uchida, M. *et al.*, 2006. Targeting of cancer cells with ferromagnetic ferritin cage nanoparticles, *J. Am. Chem. Soc.,* **128**(51), 16 626–16 633.

Walls, M.G., Cao, C., Yu-Zhang, K., Li, J., Che, R. & Pan, Y., 2013. Identification of ferrous-ferric Fe_3O_4 nanoparticles in recombinant human ferritin cages, *Microsc. Microanal.,* **19**(04), 835–841.

Walton, D., 1980. Time-temperature relations in the magnetization of assemblies of single domain grains, *Nature,* **286**(5770), 245–247.

Williams, W. & Walton, D., 1988. Thermal cleaning of viscous magnetic moments, *Geophys. Res. Lett.,* **15**(10), 1089–1092.

Wilson, R.L., 1961. The Thermal demagnetization of natural magnetic moments in rocks, *Geophys. J. Int.,* **5**(1), 45–58.

Wohlfarth, E.P., 1958. Relations between different modes of acquisition of the remanent magnetization of ferromagnetic particles, *J. Appl. Phys.,* **29,** 595–596.

Worm, H.-U. & Jackson, M., 1999. The superparamagnetism of Yucca Mountain Tuff, *J. geophys. Res.,* **104,** 25 415–25 425.

York, D., 1978a. Magnetic blocking temperature, *Earth planet. Sci. Lett.,* **39,** 94–97.

York, D., 1978b. A formula describing both magnetic and isotopic blocking temperatures, *Earth planet. Sci. Lett.,* **39,** 89–93.